PNAS
www.pnas.org

Supplementary Information for

Imaging electron-density fluctuations by multidimensional X-ray photon-coincidence diffraction

Lyuzhou Ye, Jérémy R. Rouxel, Daeheum Cho, Shaul Mukamel

Lyuzhou Ye, Shaul Mukamel
lyuzhouy@uci.edu, smukamel@uci.edu

This PDF file includes:

Supplementary text
Figs. S1 to S2

Supporting Information Text

Scattered intensities and the dominating pathways. To investigate the dynamics of the signals in momentum space, we selected a $\mathbf{q}_2$ point $[(q_y, q_z)$ for yy configuration and (q_x, q_z) for yx configuration$]$ $(-0.19\,\text{Å}^{-1}, 0.59\,\text{Å}^{-1})$ from the $\mathbf{q}_2$ scattering pattern in Fig. 4 of the main text. The corresponding time-dependent scattered intensities for pulse configurations yy and yx at two $\mathbf{q}_1$ points A and B are plotted in Fig. S1(a). The sum-over-states expression Eq. (3) allows to identify the pathways that dominate the signal. For example, at the $\mathbf{q}_1$ point A for the yy configuration in Fig. 4 of the main text, with the interaction of the two temporally separated pulses $\mathbf{k}_{p1}$ and $\mathbf{k}_{p2}$ along y, the dominating pathways $|g\rangle\langle g| \to |2\rangle\langle 2| \to |2\rangle\langle 2|$, $|g\rangle\langle g| \to |2\rangle\langle 2| \to |8\rangle\langle 8|$ and $|g\rangle\langle g| \to |3\rangle\langle 3| \to |9\rangle\langle 9|$ are time independent, because the $\mathbf{k}_{p1}$ pulse prepares the molecule in the populations. The time-independent pathways can be subtracted by looking at the signal difference $S(T) - S(T = 0)$. The time-dependence of the signal is dominated by the pathways $|g\rangle\langle g| \to |5\rangle\langle 2| \to |8\rangle\langle 8|$ and $|g\rangle\langle g| \to |6\rangle\langle 3| \to |9\rangle\langle 9|$ (and their complex conjugates).

The scattered intensities exhibit a simple time-dependent feature. The oscillation period is mainly determined by the energy differences $(E_5 - E_2)$ and $(E_6 - E_3)$, indicating that the molecule is promoted to the coherence $|5\rangle\langle 2|$ and $|6\rangle\langle 3|$ (and the complex conjugates) by the first pulse. As displayed in Fig. 1(d), the excited states E_2, E_3 and E_5, E_6 are energetically degenerate. However, it is found that the coherences $|6\rangle\langle 2|$ and $|5\rangle\langle 3|$ and their complex conjugates do not contribute to the signal. Because the corresponding transition charge densities σ_{83}, σ_{86}, σ_{92}, σ_{85} are all zero. Figure S1(b) depicts the scattered intensities for pulse configuration yx at $\mathbf{q}_1$ point A, where the oscillating behaviors are similar to those in Fig. S1(a). Analysis of the signal shows that the same scattering pathways as those in Fig. S1(a) dominate the signal, except that the time-independent pathway $|g\rangle\langle g| \to |2\rangle\langle 2| \to |2\rangle\langle 2|$ has only neglectable contributions.

The beating patterns are observed in Fig. S1(c), indicating the interference between various pathways. Analyzing signals in detail shows that two different energy differences $(E_4 - E_2)$ and $(E_5 - E_2)$ determine the oscillation period. The dominating time-dependent pathways are $|g\rangle\langle g| \to |5\rangle\langle 2| \to |2\rangle\langle 2|$ and $|g\rangle\langle g| \to |4\rangle\langle 2| \to |8\rangle\langle 8|$ (and their complex conjugates). Figure S1(d) can be analyzed similarly. It is found that the time-dependence of the signal is dominated by the pathway $|g\rangle\langle g| \to |4\rangle\langle 2| \to |8\rangle\langle 8|$ and its complex conjugate. The oscillation amplitudes for configurations yy and yx at point B are smaller compared to those for point A, because the $\mathbf{q}_1$ scattered intensity (see Fig. 2) and the dominating density matrix elements (see Fig. 3) for point B are smaller than those for points A.

Charge densities in real space. Figure S2 depicts the charge densities $\sigma_{ec}(\mathbf{r})$ that contribute to the dominating correlation functions $g_{eced}(\mathbf{R}_2)$ for the real-space signal Eq. (4) of the main text. If a pathway is time-independent, then the superposition coefficient $f_{ecc}(\mathbf{q}_1)g_{cgcg}(\mathbf{q}_1)$ is real and time-independent. Therefore, the corresponding charge-density correlation function $g_{ecec}(\mathbf{R}_2)$ appears only in the real part of the signal $S(\mathbf{q}_1, \mathbf{R}_2, T)$.

As an example, for yy configuration at $\mathbf{q}_1$ point A, the signals $\text{Im}[S(\mathbf{q}_1, \mathbf{R}_2, T)]$ are cylindrically symmetric along x, since that all the contributing transition charge densities and thus the correlation functions $g_{eced}(\mathbf{R}_2)$ possess the cylindrical symmetry along x. Due to the degeneration of the valence excited states $E_2 = E_3$, $E_5 = E_6$ and $E_8 = E_9$, the corresponding transition charge densities are identical, *i.e.* $\sigma_{82}(\mathbf{r}_2) = \sigma_{93}(\mathbf{r}_2)$ and $\sigma_{85}(\mathbf{r}_2) = \sigma_{96}(\mathbf{r}_2)$, as shown in Fig. S2. The real-space two-photon coincidence signal thus presents the dynamics of the correlation functions of the transition charge densities $g_{8582}(\mathbf{R}_2) = g_{9693}(\mathbf{R}_2)$ and $g_{8285}(\mathbf{R}_2) = g_{9396}(\mathbf{R}_2)$. This provides a real-space visualization of the time-dependent pathways that dominate the signals for yy configuration at $\mathbf{q}_1$ point A in Fig. 4.

 Lyuzhou Ye, Jérémy R. Rouxel, Daeheum Cho, Shaul Mukamel

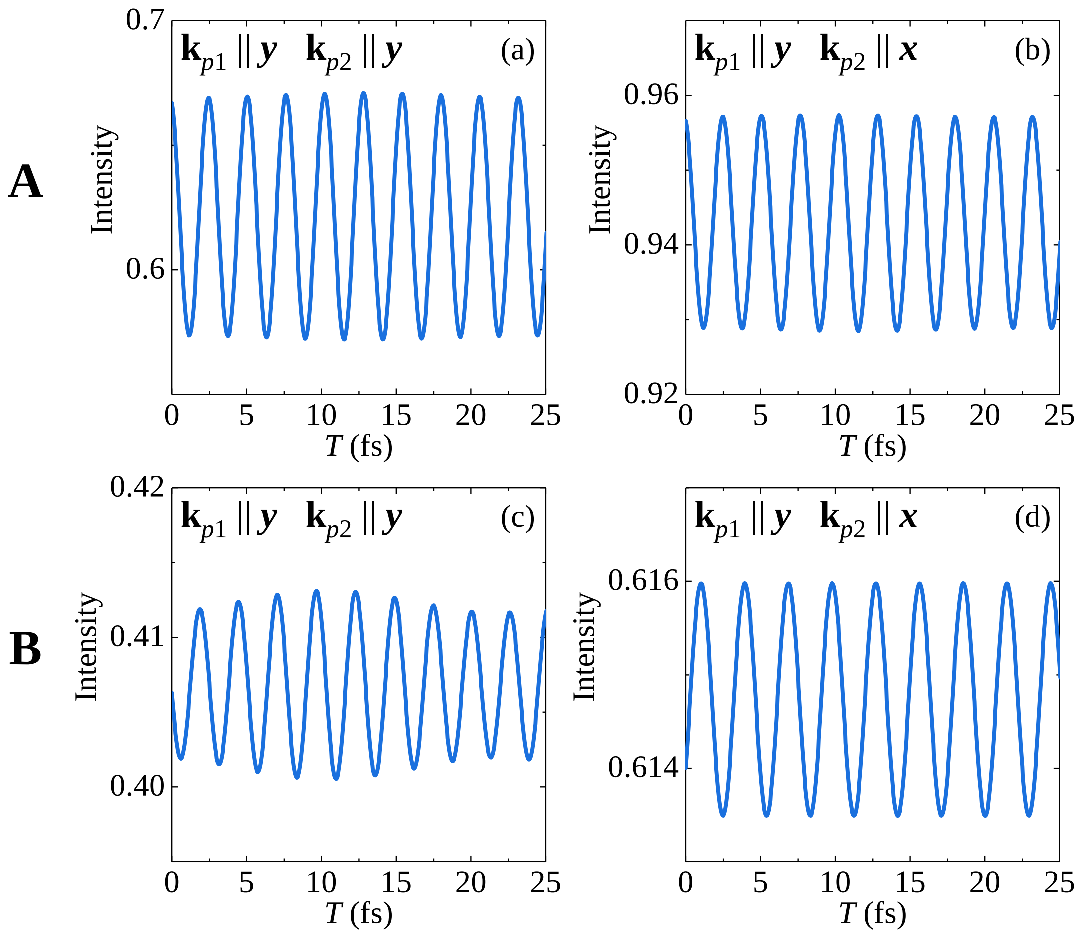

Fig. S1. The scattered intensities Eq. (3) as a function of time delay T at the $\mathbf{q}_2$ point $(-0.19\,\text{Å}^{-1}, 0.59\,\text{Å}^{-1})$ in Fig. 4 of the main text.

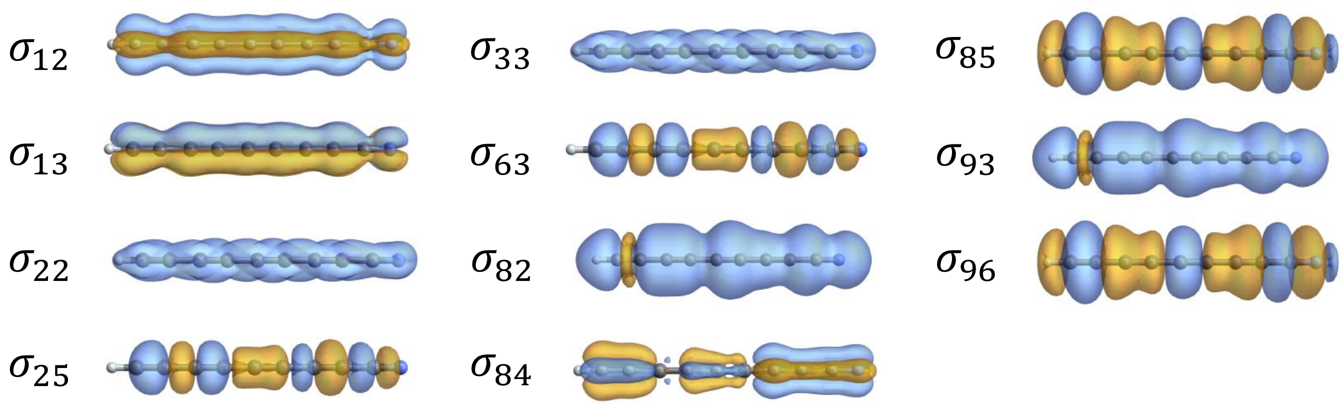

Fig. S2. The charge densities $\sigma_{ec}(\mathbf{r})$ that contribute to the dominating correlation functions $g_{eced}(\mathbf{r})$.